https://doi.org/10.1016/j.matdes.2015.12.055

Surface damage mechanism of WC/Co and RB-SiC/Si composites under high spindle speed grinding (HSSG)

Quanli Zhang[1,2], Suet To[2]*, Qingliang Zhao[1] and Bing Guo[1]

[1] Centre for Precision Engineering, School of Mechatronics Engineering, Harbin Institute of Technology, Harbin, 150001, China

[2] State Key Laboratory of Ultra-precision Machining Technology, The Hong Kong Polytechnic University, Hong Kong, China

*Corresponding Author / E-mail: sandy.to@inet.polyu.edu.hk, TEL: +852-2766 6587, FAX: +852-2764 7657

Abstract The surface damage mechanisms of WC/Co and Reaction-bonded SiC/Si (RB-SiC/Si) composites under high spindle speed grinding (HSSG) were investigated in the present work. Sharp edge loss and grit splintering were identified as two typical diamond wheel wear mechanisms. Plastic scratching grooves, Co extrusion and WC dislodgement were generated on the machined surface of WC/Co after grinding, while micro-pits of varied sizes at the phase boundaries and plastic scratching grooves were the main surface characteristics for RB-SiC/Si. Moreover, it was found that non-uniform surface finish at different radial positions resulted from the increase in material removal rate for both WC/Co and RB-SiC/Si, and the simulated results based on Soneys' model mostly corresponded with the measured outcomes. In addition, obvious relative wheel-workpiece vibration induced surface waviness was found, and its effect on the surface profile was analyzed for the wheel edge profile considered, which differed with that from single point diamond machining (SPDT).

Keywords: High spindle speed grinding (HSSG); Plastic deformation; Fracture; Vibration; Surface finish

1. Introduction

With the strong demand for high mechanical properties at elevated temperature and in severe environments, hard materials are gaining expanding applications in aeronautics and astronautics, optical moldings and the nuclear industry [1, 2]. Silicon carbide (SiC) and tungsten carbide (WC) are two typical materials that have been widely used due to their high strength and hardness, good corrosion resistance and chemical stability [3-5]. To further improve the properties of bulk materials, specific dopants are added in processing stage [3, 6]. The reactive infiltration of liquid Si with SiC and the Co reaction with WC can greatly improve their toughness and density [7, 8].

However, a great challenge still exists in machining these materials to achieve optical surface quality. Ultra-precision grinding is regarded as one of the most appropriate methods to machine these types of ceramics and has been widely used to optimize the processing parameters to achieve superior surface finish. For the grinding of ceramics and glasses, a number of studies have focused on the material removal mode [9-12] and surface integrity [13-15]. More specifically, it was found that typical surface characteristics are plastic scratching grooves for WC/Co and brittle fracture for RB-SiC/Si carbides under grinding [15-20], respectively, attributed to their varied mechanical properties. However, the impact of binders on surface formation still needs further consideration. Moreover, it was believed that the material removal rate, a combination of different processing parameters, played a determinant role on the surface quality that could be achieved [2, 21]. Different mathematical models were built to investigate the influence of the material removal rate [15, 22, 23]. Nevertheless, previous works seemed to pay less attention to the non-uniform surface finish of a certain workpiece, which is closely related to the surface damage mechanism. Actually, it could have resulted from the varied material removal rate at different positions of a certain workpiece,

which would yield greater impact on performance. Furthermore, in the high spindle speed machining process, the relative vibration between the tool and workpiece would inevitably affect the surface quality [24, 25]. For instance, Cheung and Lee [26] found that the vibration amplitude between the tool and workpiece limited the surface quality achieved, while Zhang and To [27, 28] showed that spindle vibration could affect the surface profile and cutting force in ultra-precision raster milling and diamond turning. For grinding, the impact of wheel chatter and vibration on the surface roughness and form accuracy were both identified [29-34], however, there is still a lack of direct research on the surface characteristics generated under relative wheel-workpiece vibration.

Based on the above discussion, high spindle speed grinding (HSSG) of WC/Co and RB-SiC/Si composites was conducted to investigate the different influencing factors on the surface damage mechanism. Firstly, the profile and surface morphology of the diamond wheel after dressing and grinding were examined, after which the non-uniform surface finish at different radial positions on the machined surface was investigated. In addition, indentation test was performed on the polished surface, the results of which could provide us a basic knowledge of the damage mechanism for WC/Co and RB-SiC/Si under quasi-static pressure and help to explain the results in high spindle speed grinding (HSSG). Finally, the impact of relative wheel-workpiece vibration on the surface topography was characterized and analyzed.

2. Experimental procedures

2.1 Materials and methods

Micro-grinding of RB-SiC/Si and WC/Co was performed on a three axes ultra-precision grinding machine (450UPL, Moore Nanotech. USA). An illustration of the grinding setup is shown in Fig.1 (a). The parallel grinding mode was utilized in this study, with the feed direction along the X axis and the depth of

grinding controlled by Z axis, as shown in Fig.1 (b). A diamond wheel of 1500# grit size (Diagrind, Inc., USA) was used after appropriate truing by a diamond nib.

In ultra-precision grinding of hard and brittle materials, the aim is to achieve a nanometric surface finish to meet the requirement of optical surface quality. However, it was found that the average surface roughness (R_a) of both RB-SiC/Si and WC/Co composites were limited to be around 20 nm and 8 nm, respectively, even with much finer parameters (grinding depth:0.1 μm, feed rate: 0.1 mm/min). In the present work, we focus on the study of the grinding induced surface damage mechanism for WC/Co and RB-SiC/Si composites so only the optimal machining parameters (grinding depth:0.5 μm, feed rate: 0.5 mm/min) were chosen, with the machining efficiency taken into consideration. Moreover, to reduce the impact of vibration on surface roughness, the tool rotational speed was chosen to be 20,000 *RPM*. The detail grinding parameters are tabulated in Table 1.

Table 1. Detail grinding and truing parameters

Grinding	$1500^{\#}$ W/60° diamond wheel	diam. 20 mm, resin bonded
	Grinding width B (μm)	150
	Wheel RPM n_s (rpm)	20,000
	Workpiece RPM n_w (rpm)	120
	Feed rate f (mm/min)	0.5
	Depth of grinding a_e (μm/pass)	0.5
Truing	Truer	Diamond nib
	Feed rate (mm/min)	5
	Depth of truing (μm/pass)	5
	Truer RPM (rpm)	300
	Wheel RPM (rpm)	2000
Coolant	CLAIRSOL 350	MQL

The indentation test was conducted on the polished original material surfaces by Vickers micro-hardness tester (MicroWiZhard), under a load of 0.1 kg, with a loading time of 5 s, holding time of 10 s and unloading time 5 s. Indentation tests were repeated three times for both WC/Co and RB-SiC/Si at varied

surface positions, to investigate the surface damage generated under quasi-static normal pressure.

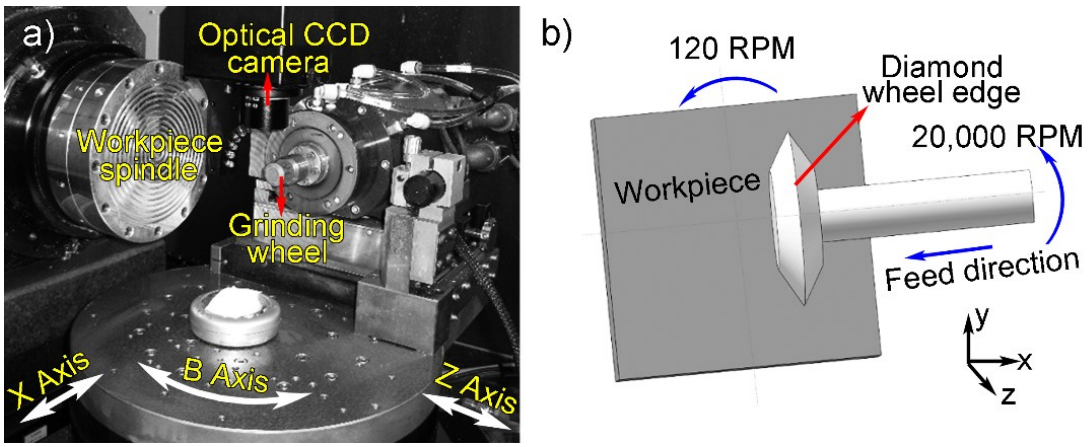

Fig. 1. Illustration of the (a) grinding setup; (b) parallel grinding mode

Commercially available WC and RB-SiC carbides (Goodfellow Cambriage Ltd., UK) was machined and the detail mechanical properties are listed in Table 2.

Table 2. Workpiece materials properties

Bulk Workpiece	RB-SiC/Si	WC/Co
Elastic modulus E (GPa)	410	600
Vikers hardness H (kg/mm^{-2})	2500	1550
Fracture toughness K_{IC} (MPa m$^{1/2}$)	3.0 [19] and [20]	11.0 [35]
Compressive strength (MPa)	2000	5500
Binder content (wt.%)	Si~10.0	Co~6.0
Density ρ (g/cm^3)	3.1	14.95
Size of workpiece (mm)	16×16×5	12×12×5

2.2 Characterization

The wheel surface morphology was measured by scanning electron microscope (SEM, Hitachi TM3000) after truing and grinding, while the surface topography of the worn edge was examined by a 3D optical measuring system (Alicona IFM G4). The indents and the grinding surface were characterized by optical microscopy (Olympus BX60), and the machined surface was also examined by a scanning electron microscope (SEM, Hitachi TM3000) and an atomic force microscope (AFM, Park's XE-70) to analyze the surface characteristics. White light interferometers (Wyko NT8000 and Zygo Nexview) were used to

measure the surface roughness and cross-sectional profile of the grinding surface. The data achieved was processed by Vision.exe program (Veeco Instruments Inc., USA), installed on Wyko NT8000.

3. Results and discussion

3.1 Wear of diamond wheel

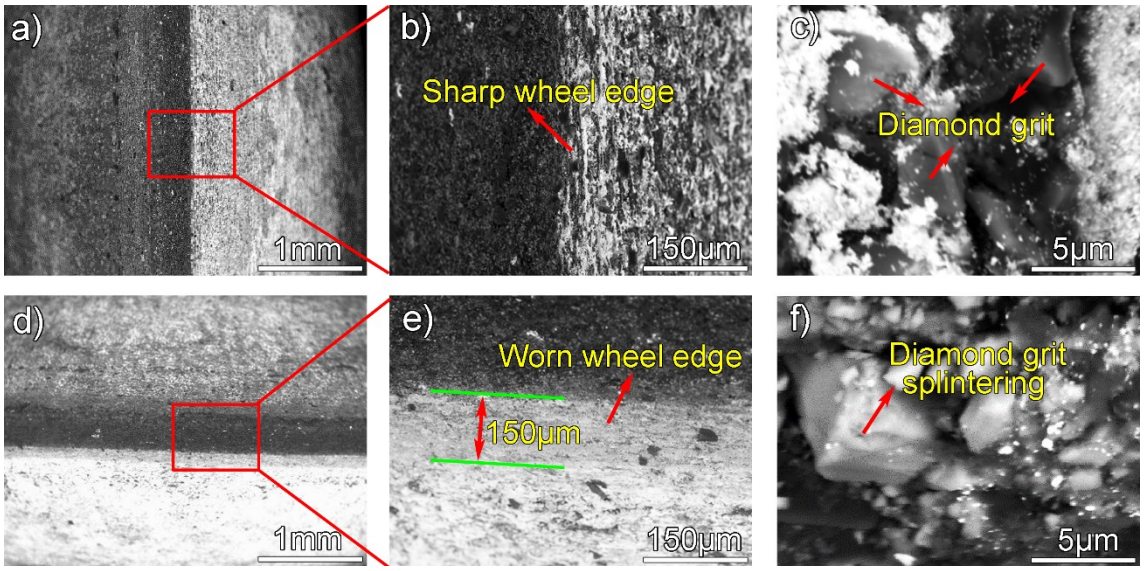

Fig. 2. The grinding edge profile of the 1500# diamond wheel: (a), (b) and (c) after truing measured by SEM; (d), (e) and (f) after grinding WC/Co measured by SEM

As is well known, the surface quality of a ground workpiece achieved is determined by the wheel topography, so appropriate truing and dressing of the grinding wheel before and during the machining process is a prerequisite for achieving superior surface finish [14, 36]. Fig. 2(a) and (b) show the sharp edge profile of the diamond wheel obtained by truing with the diamond nib. In addition, the diamond grits protruded out of the resin bond, as is shown in Fig. 2(c). The original workpiece surface was firstly ground to be a flat under the machining parameters (grinding depth: 0.5 μm， feed rate: 0.5 mm/min). As is known, the diamond wheel wear and surface damage of the workpiece will be induced during this stage. Therefore, a re-truing process was performed, and 10 passes of grinding were conducted to eliminate the impact of

previous surface defects. However, wear of this sharp edge still occurred during grinding of WC/Co and RB-SiC/Si carbides, as shown in Fig. 2(d). Specifically, the grinding width which was responsible for surface formation was around 150 μm measured by SEM after grinding, as illustrated in Fig. 2(e), and splintering of the diamond grits appeared on the cutting edge, which can be seen from Fig. 2(f). The average grits diameter was calculated to be 3.7 μm according to [33], which can also be estimated from Fig. 2(c), less than the feed per revolution (4.17 μm). Furthermore, it can be readily seen that the protruded heights of diamond grits are not uniform, as shown in Fig. 3. Removal of the resin bond around it would also promote the dislodgement of grits if the protrusion height became greater than half the grit diameter.

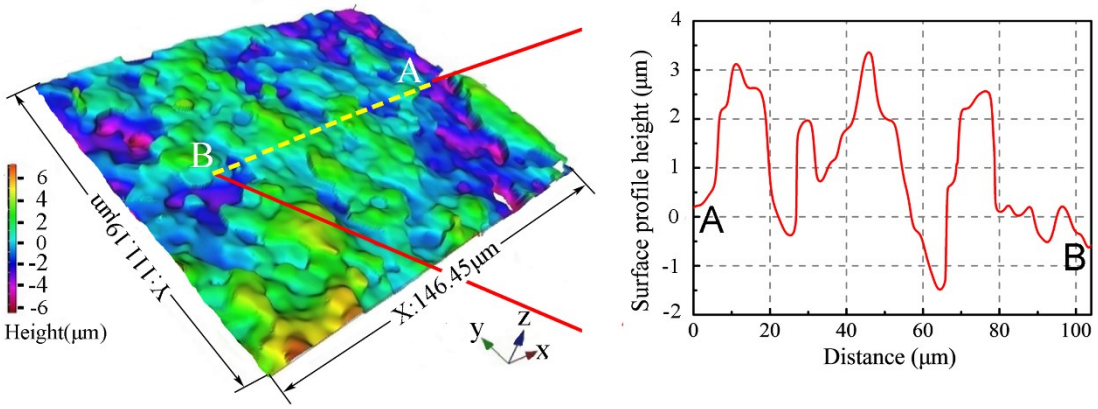

Fig. 3. Surface topography and cross-sectional profile of the worn wheel edge after grinding

3.2 Behavior of material under indentation

As can be seen from Fig. 4, only regular indentation dimples were replicated from the Vickers indenter on the WC/Co surface, and there were no cracks generated near the indentation position. Under the pressure of the indenter, the workpiece material was extruded and swelled out at the edge. For RB-SiC/Si at the same loading force, obvious radial cracks were found around the four sharp tips. The average particle size of WC and SiC was ~2 μm and ~10 μm, respectively. Compared with WC/Co, the coarser grain size of RB-SiC/Si and non-uniform distribution of the SiC particles would cause

greater stress concentration at the phase boundaries. Therefore, lateral cracks were prone to form and extend along the phase boundaries, resulting in chipping of the surface.

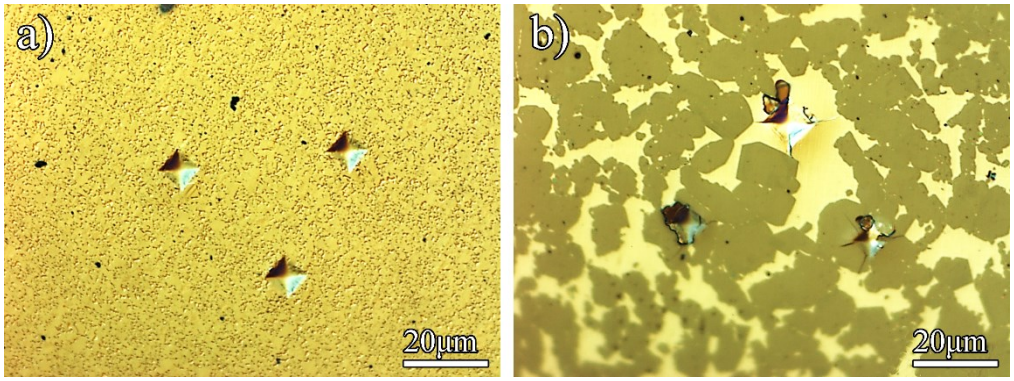

Fig. 4. Vickers-hardness indentation profile under 0.1 kg: (a) WC/Co; (b) RB-SiC/Si

3.3 Role of material removal rate

3.3.1 Theoretical methodology

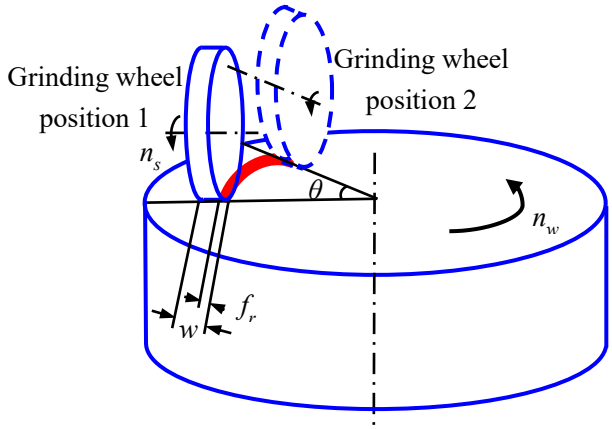

Fig. 5. Illustration of the material removal for parallel grinding

The width of the worn grinding edge (w) is about 150 μm (see Fig. 2(e))，much larger than the feed rate per revolution (f_r=4.17 μm). As is illustrated in Fig. 5, the material removal rate (Q_w) is dependent on the feed rate as $w > f_r$. The material removal rate is expressed as follows [37, 38]:

$$Q_w = a_e \cdot v_w \cdot f_r = a_e \cdot \frac{\pi \cdot d \cdot n_w}{1000 \times 60} . f_r \quad (1)$$

Then, the tangent grinding force is given as [39]:

$$F_t = \frac{e_c \cdot Q^{'} \cdot b_w}{v_s} = \frac{e_c \cdot Q_w}{v_s} \tag{2}$$

where a_e is the grinding depth, v_w is the workpiece speed, d is the distance from the center, n_w is the rotation speed of the workpiece, v_s is the wheel speed, f_r is the feed per revolution, e_c is the specific grinding energy, Q' is the specific material removal rate, b_w is the grinding width. From the above equations, v_w was variable at different radial position of the workpiece.

Snoeys et al. [40, 41] proposed an empirical surface roughness model related to the undeformed chip thickness, expressed as follows:

$$R_a = R_1 \cdot \left(\frac{v_w \cdot h_{\max}}{v_s} \right)^x \tag{3}$$

Where R_1 and x are two constants depending on the particular experiment. h_{max} is the unformed chip thickness which has been frequently employed to explain the material removal mode during machining of hard and brittle materials, and the following expression [33] was used in the present work:

$$h_{\max} = \left[\frac{4}{Cr} \left(\frac{v_w}{v_s} \right) \left(\frac{a_e}{d_{se}} \right)^{1/2} \right]^{1/2} \tag{4}$$

in which, d_{se} is the equivalent diameter of the wheel, C is the grit surface density and r is the ratio of the chip width to the average undeformed chip thickness.

3.3.2 Effect on surface morphology

The surface morphology of WC/Co and RB-SiC/Si carbides after grinding is shown in Fig. 6. The surface of WC/Co was mainly covered by obvious plastic grinding grooves, while surface fracture occurred on RB-SiC/Si, except the plastic grinding grooves. This is consistent with the indentation test. In the center of WC/Co and RB-SiC/Si, a certain residual height of workpiece material remained on the machined surface, and a circle of plastic stripes formed on WC/Co at about 50 μm from the center, whereas a circle of surface

fragmentation appeared on RB-SiC/Si. This was attributed to the machine position error and macro wheel wear in the previous studies [42, 43]. Above all, it could be readily found that the surface quality deteriorated with increasing distance from the center for both WC/Co and RB-SiC/Si carbides. According to equations (1) and (2), the stock material removal rate increased with the increase of v_w, resulting in a higher grinding force. Greater plastic deformation and brittle fracture were produced, which directly affected the surface quality.

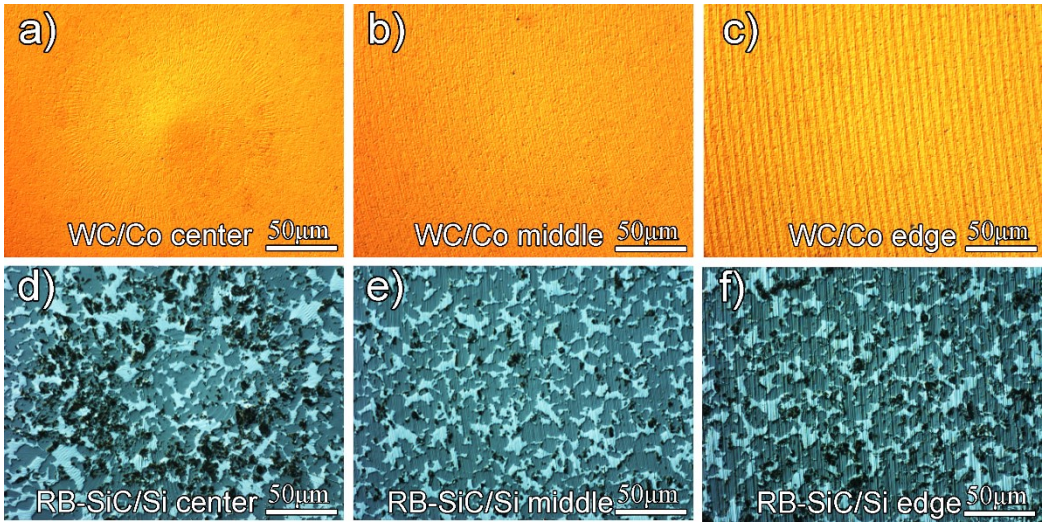

Fig. 6. Morphology of the machined WC/Co and RB-SiC/Si surface at different radial position: (a) WC/Co center, (b) WC/Co middle and (c) WC/Co edge position; (d) RB-SiC/Si center, (e) RB-SiC/Si middle and (f) RB-SiC/Si edge position

To illustrate the surface damage induced by high spindle speed grinding (HSSG), the surface morphology and topography measured by SEM and AFM are shown in Fig. 7, compared with the polished original material surfaces. From Fig. 7(a) and (d), it can be seen that both the WC/Co and RB-SiC/Si carbides are densified with the addition of Co and Si, respectively, without any obvious defect on the polished surface. As shown in Fig. 7 (b), apart from the grinding induced plastic deformation, the machined surface of WC/Co appears to become compacted, where the mean free path of cobalt binder reduced in the

grinding direction, indicating the Co binder being extruded under the pressure of diamond grits. Under the random scratching of diamond grits, the extruded Co will be segmented into small parts, resulting in the formation of many protrusions, as shown in Fig. 7(c). In addition, some WC grains were also dislodged under the dynamic pressure of the diamond grits. For RB-SiC/Si, there were also many plastic grooves on the surface after grinding. However, a great number of micro-pits occurred and were distributed randomly near the phase boundaries in the grinding direction, which are shown in Fig. 7(e) and (f). This is consistent with the indentation test, which indicates that coarse grains induced strain concentration at phase boundaries of RB-SiC/Si make them more fragile under both quasi-static and dynamic pressure.

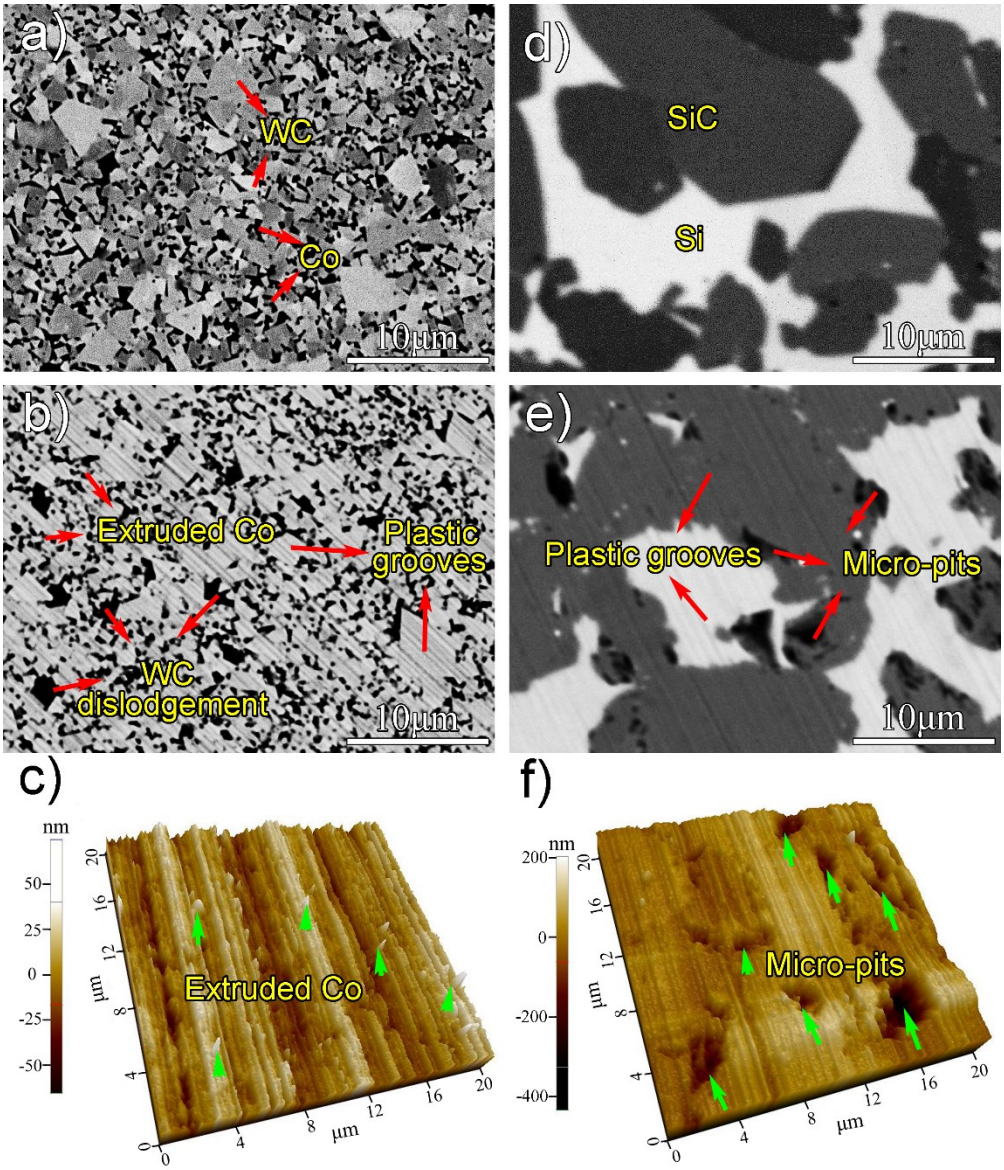

Fig. 7. (a) and (b) SEM morphology of the polished and machined WC/Co carbide; (c) Surface topography of the machined WC/Co measured by AFM; (d) and (e) SEM morphology of the polished and machined RB-SiC/Si carbide; (f) Surface topography of the machined RB-SiC/Si measured by AFM

3.3.3 Surface roughness

Fig. 8 shows that surface roughness increases slowly with increasing radial distance from the center for both WC/Co and RB-SiC/Si carbides. As mentioned above, the only variable was the velocity at different radial distances from the center, so it should account for the non-uniform surface finishes at different radial positions. Based on the results of a series of experiments conducted to optimize the

machining parameters, R_1 and x were experimentally determined to be 1.5 and 0.32, respectively. Using the surface morphology, topography and the cross-sectional profile of the diamond wheel, C was calculated to be 55. In the present work, considering the specific grinding depth (0.5 μm), it is important to point out that C is calculated for grits with a certain protrusion heights, as only these grits are of great possibility to be engaged in material removal. Therefore, there might be some errors in calculating the values of C. While for r, a value of 90 for the ultra-fine diamond wheel was used following Wobker and Tonshoff [44, 45]. The simulated results were also shown in Fig. 8. According to the reference [43], a stepped grinding edge profile of the diamond wheel (corresponding to primary material removal zone and secondary material removal/finish zone) was generated in parallel grinding mode when the radial feed per revolution (f_r=4.17 μm) is much lower than the grinding width (worn edge width: 150 μm). For a certain workpiece machined under the constant parameters, the smaller distance from the center means the more obvious effects of the secondary finish zone, resulting in a gradual improvement of the surface finish. Therefore, the wear of diamond wheel also contributed to the non-uniform surface finish for a certain workpiece. However, the effect is insignificant compared with the impact of surface fracture occurred for RB-SiC/Si and hard particle dislodgement for WC/Co, as shown in Fig. 7. Except for the great difference of the surface roughness value in the center, caused by position error and macro wheel wear [42, 43], the trend of the measured results and simulation agreed but the values differed, especially for RB-SiC/Si. As is known, variable chip thickness in grinding results from the random protruded height of diamond grits, so using a grinding depth of 0.5 μm in the simulation would lead to differences with the experimental results. In addition, based on the above analysis, the experimentally determined values of R_1 and x, the calculated C based on a small surface area of wheel, and the reference value of r could all induce some errors in the simulation. Therefore, the choice

of R_1, x, C and r also affects the final results. Furthermore, the material properties should be considered as a further reason for the difference between WC/Co and RB-SiC/Si, as all the grinding parameters were the same. Finally, the relative tool-workpiece vibration would increase the surface waviness, as well as the surface roughness.

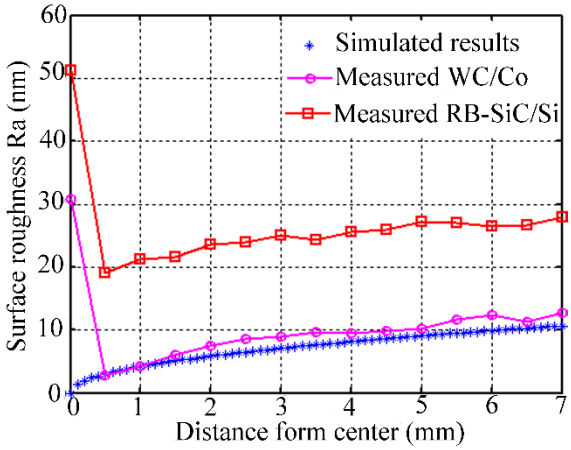

Fig. 8. Simulated and measured surface roughness R_a plotted against radial distance from center

3.4 Role of vibration

3.4.1 Vibration induced surface characteristic

Fig. 9 shows the typical 3D morphology and the respective cross-sectional profile of the machined WC/Co and RB-SiC/Si surfaces at a distance of 6 mm from center. It was found that the surface waviness was more uniform for WC/Co compared with RB-SiC/Si, with the amplitude being around 0.08 μm and 0.35 μm, respectively. Besides, the vibration induced marks could be readily observed due to the plastic deformation on WC/Co. Nevertheless, the same phenomenon was not so clear on RB-SiC/Si due to the random surface fractures.

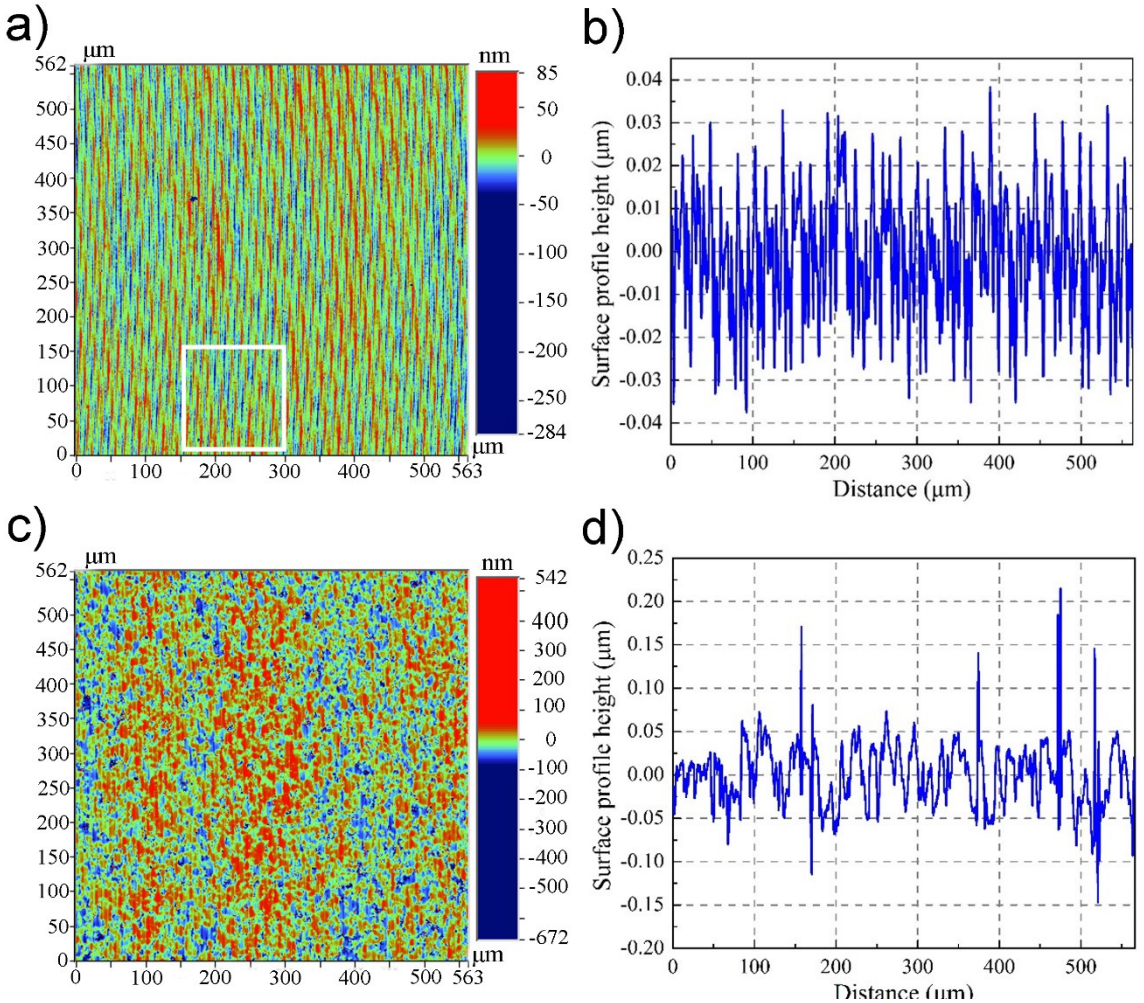

Fig. 9. Typical surface topography and cross-sectional surface profile: (a) and (b) for WC/Co; (c) and (d) for RB-SiC/Si

To get further insight into the influence of the wheel-workpiece vibration, original surface profile data at a radial distance of about 6 mm from the center was measured by Zygo Nexview and then processed by low pass Fourier filtering with Vision.exe software, as shown in Fig. 10(a). The measured peak distance was about 298 µm, corresponding to a radial spatial frequency of 3.35 1/mm. In addition, an enlarged sub-region of the WC/Co surface was taken from Fig. 9(a), and shown in Fig. 10(b). Different peak distances can be identified and assigned with Arabic numbers in Fig. 10(b). With the help of the Vision.exe software, the peak distances d_{pp} were calculated to be about 20 µm, 11 µm, 7 µm, 4 µm and 3µm, respectively. Based

on the measured waviness peak values d_{pp}, the spatial frequency $f_{spatial}$ can be calculated by following equation:

$$f_{spatial} = \frac{1}{d_{pp} \times 10^{-3}} \tag{5}$$

$f_{spatial}$ was calculated to be 50, 90.9, 142.85, 250 and 333 1/mm, accordingly. It can also be seen that the peak height between ①, ②, ③ was more noticeable compared with ④ and ⑤.

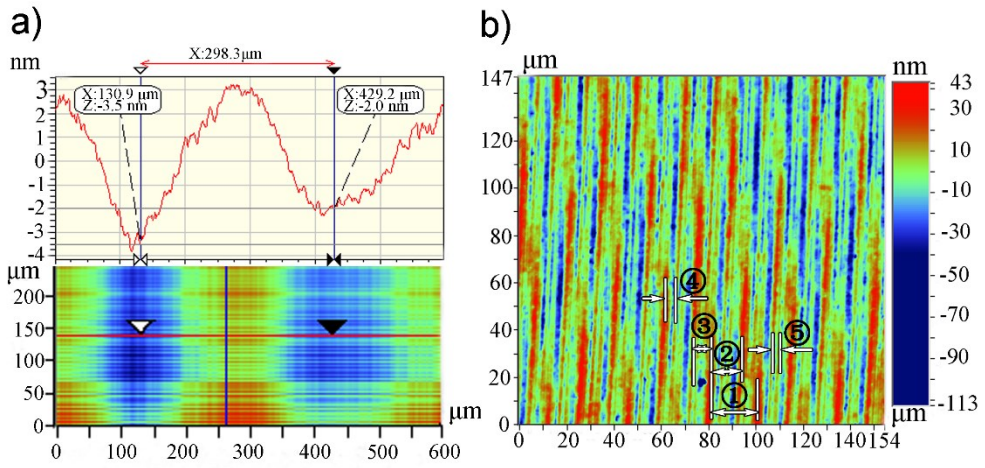

Fig. 10. WC/Co surface profile: (a) Radial vibration after being dealt with the low pass Fourier filtering; (b) Circular vibration in enlarged sub-region

3.4.2 Analysis of vibration induced surface characteristics

To analyze the different influencing factors on the surface waviness profile, the surface cross-sectional profile data was processed by a Fast Fourier Transform (FFT) based Matlab program. As shown in Fig. 11, varied spatial frequencies (55, 90, 145, 238, and 293 1/mm) appeared at even the same position for both WC/Co and RB-SiC/Si carbides. As reported by Cheung and Lee [26], adjacent vibration cycles and the phase shift ϕ of the vibration would affect the calculated spatial frequency outcomes, marked by ①, ② and ③ in Fig.10(b). The calculated results by equation (5) corresponded with the values obtained using the power spectrum method. The phase shift frequency of tool-workpiece vibration $v_{t,w}$ on the workpiece

was given by Cheung [46]:

$$\phi = 2\pi\varepsilon, -0.5 \le \varepsilon \le 0.5 \tag{6}$$

$$v_{t,w} = \frac{\phi}{2\pi \cdot f_r} \tag{7}$$

Furthermore, the tool feed effect on the surface characteristic should be considered. According to [47], the following tool feed frequency $v_{F1,nf}$ equation on workpiece was proposed:

$$v_{F1,nf} = \frac{(n_f + 1)}{f_r}, \text{ for } n_f = 0, 1, 2 \ldots \tag{8}$$

In single point diamond turning, only when the tool nose radius was smaller than feed rate could the feed components be observed clearly [47]. However, in the present study, the measured grinding width of diamond wheel was 150 μm (see Fig. 2), much larger than the feed per revolution (4.17μm/r), so the wheel feed does not contribute to the feed component if the wheel edge is regarded in its entirety. Nevertheless, things became different when the diameter of single diamond grit (3.7 μm) is taken into consideration. Therefore, the diamond grits would contribute to the formation of feed components in the tool feed for the power spectral density of spatial frequency, marked ④. Moreover, the random distribution of the diamond grits in grinding wheel contributed to the varied grit scratching grooves in the same grinding pass, marked ⑤. So it resulted in an inconsistency between the calculated spatial frequency $f_{spatial}$ with the power spectral analysis result. Some obvious spatial frequency lower than 50 1/mm peaks also appeared. This was attributed to the surface micro-pits caused by the dislodgement of WC and the surface fragmentation at the phase boundaries for RB-SiC/Si [48].

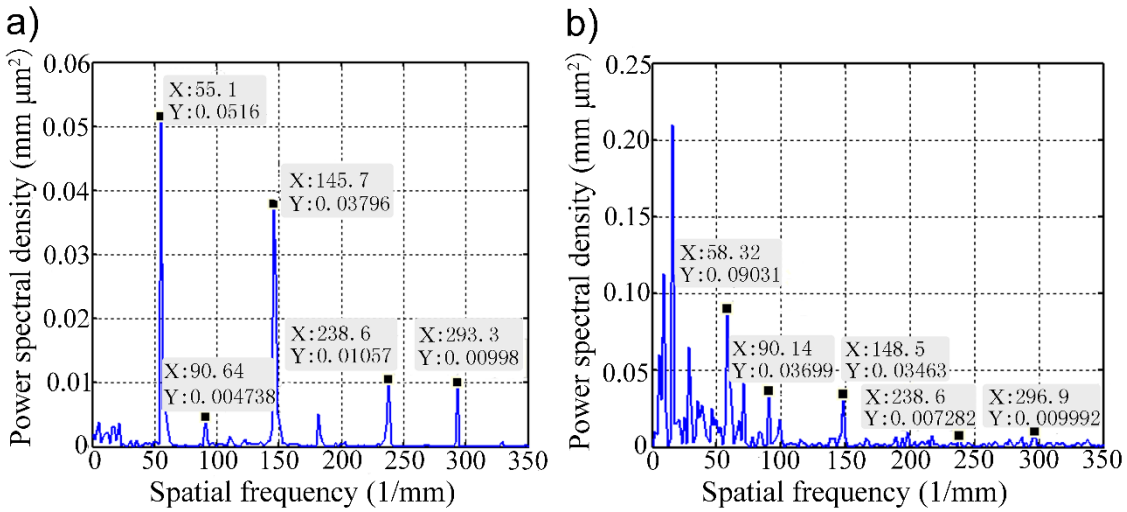

Fig. 11. Power spectral densities of the surface profiles for: (a) WC/Co; (b) RB-SiC/Si

4. Conclusions

High spindle speed grinding (HSSG) of WC/Co and RB-SiC/Si carbides under optimal parameters was conducted to investigate the surface generation mechanism. Based on the above analysis and discussion, the following conclusions were reached:

(1) Different wheel wear mechanisms were observed: macro wheel wear was mainly sharp edge flattening but it did not affect the tool feed surface waviness, while the micro wear was in the form of grit splintering and dislodgement;

(2) The machined surface was characterized by plastic deformed grinding grooves, extruded Co and WC dislodgement for WC/Co, while scratching grooves and surface fracture at the phase boundaries for RB-SiC/Si;

(3) Non-uniform surface finish resulted from the varied material removal rate. The surface roughness increased with increasing radial distance from the workpiece center for both WC/Co and RB-SiC/Si carbides. The trend corresponded with the simulation results based on Soneys' model, but with some disparity;

(4) Relative tool-workpiece vibration on the grinding surface was identified, and different spatial frequencies were analyzed. Radial and circular wheel-workpiece vibration marks were influenced by the tool feed and phase shift. Considering the random distribution and diameter of diamond grits in wheel, the tool feed component during grinding differed with single point diamond machining.

In future work, investigation on the control of vibration and uniform material removal rate to eliminate non-uniform surface finish should be undertaken.

Acknowledgement

The work was supported by the Research Committee of the Hong Kong Polytechnic University (RTRA) and also the National Natural Science Foundation of China (NSFC) (Project No.:51475109).

References

[1] G. Xiao, S. To, G. Zhang, The mechanism of ductile deformation in ductile regime machining of 6H SiC, Comp. Mater. Sci. 98 (2015) 178-188.

[2] X. Wang, X. Zhang, Theoretical study on removal rate and surface roughness in grinding a RB-SiC mirror with a fixed abrasive, Appl. Optics 48 (2009) 904-910.

[3] H. Liang, X. Yao, H. Zhang, X. Liu, Z. Huang, Friction and wear behavior of pressureless liquid phase sintered SiC ceramic, Mater. Design 65 (2015) 370-376.

[4] B. Meng, F. Zhang, Z. Li, Deformation and removal characteristics in nanoscratching of 6H-SiC with Berkovich indenter, Mat. Sci. Semicon. Proc. 31 (2015) 160-165.

[5] R. Bo, S. Shaobai, L. Yawei, X. Yibiao, Effects of oxidation of SiC aggregates on the microstructure and properties of bauxite–SiC composite refractories, Ceram. Int. 41 (2015) 2892-2899.

[6] N.P. Padture, In Situ-Toughened Silicon Carbide, J. Am. Ceram. Soc. 77 (1994) 519-523.

[7] N.R. Calderon, M. Martínez-Escandell, J. Narciso, F. Rodríguez-Reinoso, The combined effect of porosity and reactivity of the carbon preforms on the properties of SiC produced by reactive infiltration with liquid Si, Carbon 47 (2009) 2200-2210.

[8] Z.Z. Fang, X. Wang, T. Ryu, K.S. Hwang, H.Y. Sohn, Synthesis, sintering, and mechanical properties of nanocrystalline cemented tungsten carbide-A review, Int. J. Refract. Met. H. 27 (2009) 288-299.

[9] Z. Liang, X. Wang, Y. Wu, L. Xie, L. Jiao, W. Zhao, Experimental study on brittle–ductile transition in elliptical ultrasonic assisted grinding (EUAG) of monocrystal sapphire using single diamond abrasive grain, Int. J. Mach. Tools Manu. 71 (2013) 41-51.

[10] T.G. Bifano, T.A. Dow, R.O. Scattergood, Ductile-Regime Grinding: A new technology for machining brittle materials, J. Manuf. Sci. Eng. 113 (1991) 184-189.

[11] M. Chen, Q. Zhao, S. Dong, D. Li, The critical conditions of brittle–ductile transition and the factors influencing the surface quality of brittle materials in ultra-precision grinding, J. Mater. Process. Technol. 168 (2005) 75-82.

[12] E. Brinksmeier, Y. Mutlugünes, F. Klocke, J.C. Aurich, P. Shore, H. Ohmori, Ultra-precision grinding, CIRP Ann. - Manuf. Technol. 59 (2010) 652-671.

[13] Q. Zhao, Y. Liang, D. Stephenson, J. Corbett, Surface and subsurface integrity in diamond grinding of optical glasses on Tetraform ‘C’, Int. J. Mach. Tools Manu. 47 (2007) 2091-2097.

[14] Q. Zhao, B. Guo, Ultra-precision grinding of optical glasses using mono-layer nickel electroplated coarse-grained diamond wheels. Part 2: Investigation of profile and surface grinding, Precis. Eng. 39 (2015) 67-78.

[15] B. Zhang, T.D. Howes, Subsurface Evaluation of Ground Ceramics, CIRP Ann. - Manuf. Technol. 44

(1995) 263-266.

[16] Y.H. Ren, B. Zhang, Z.X. Zhou, Specific energy in grinding of tungsten carbides of various grain sizes, CIRP Ann. - Manuf. Technol. 58 (2009) 299-302.

[17] H. Suzuki, M. Okada, Y. Yamagata, S. Morita, T. Higuchi, Precision grinding of structured ceramic molds by diamond wheel trued with alloy metal, CIRP Ann. - Manuf. Technol. 61 (2012) 283-286.

[18] T. Bletek, F. Klocke, M. Hünten, O. Dambon, Dressing of fine grained diamond grinding wheels for ultraprecision grinding of structured molds in brittle hard materials, Optifab, 2013, pp. 888405-888408.

[19] S. Agarwal, P.V. Rao, Experimental investigation of surface/subsurface damage formation and material removal mechanisms in SiC grinding, Int. J. Mach. Tools Manu. 48 (2008) 698-710.

[20] S. Agarwal, P. Venkateswara Rao, Grinding characteristics, material removal and damage formation mechanisms in high removal rate grinding of silicon carbide, Int. J. Mach. Tools Manu. 50 (2010) 1077-1087.

[21] F.L. Zhang, P. Liu, L.P. Nie, Y.M. Zhou, H.P. Huang, S.H. Wu, H.T. Lin, A comparison on core drilling of silicon carbide and alumina engineering ceramics with mono-layer brazed diamond tool using surfactant as coolant, Ceram. Int. 41 (2015) 8861-8867.

[22] A. Venu Gopal, P. Venkateswara Rao, Selection of optimum conditions for maximum material removal rate with surface finish and damage as constraints in SiC grinding, Int. J. Mach. Tools Manu. 43 (2003) 1327-1336.

[23] P.V.S. Suresh, P. Venkateswara Rao, S.G. Deshmukh, A genetic algorithmic approach for optimization of surface roughness prediction model, Int. J. Mach. Tools Manu. 42 (2002) 675-680.

[24] S.J. Zhang, S. To, G.Q. Zhang, Z.W. Zhu, A review of machine-tool vibration and its influence upon

surface generation in ultra-precision machining, Int. J. Mach. Tools Manu. 91 (2015) 34-42.

[25] S.J. Zhang, S. To, S.J. Wang, Z.W. Zhu, A review of surface roughness generation in ultra-precision machining, Int. J. Mach. Tools Manu. 91 (2015) 76-95.

[26] C.F. Cheung, W.B. Lee, Study of factors affecting the surface quality in ultra-precision diamond turning, Mater. Manuf. Process. 15 (2000) 481-502.

[27] S.J. Zhang, S. To, A theoretical and experimental study of surface generation under spindle vibration in ultra-precision raster milling, Int. J. Mach. Tools Manu. 75 (2013) 36-45.

[28] S.J. Zhang, S. To, A theoretical and experimental investigation into multimode tool vibration with surface generation in ultra-precision diamond turning, Int. J. Mach. Tools Manu. 72 (2013) 32-36.

[29] I. Inasaki, B. Karpuschewski, H.S. Lee, Grinding chatter - origin and suppression, CIRP Ann. - Manuf. Technol. 50 (2001) 515-534.

[30] H.K. Toenshoff, B. Kuhfuss, Influence of mechanical vibrations on workpiece shape in external plunge grinding. SME Manuf. Eng. Trans. (1984) 352-358.

[31] J.F.G. Oliveira, T.V. França, J.P. Wang, Experimental analysis of wheel/workpiece dynamic interactions in grinding, CIRP Ann. - Manuf. Technol. 57 (2008) 329-332.

[32] R. Snoeys, D. Brown, Dominating parameters in grinding wheel and workpiece regenerative chatter. Adv. Mach. Tool Des. Res. (2013) 325-348.

[33] S. Malkin, C. Guo, Grinding technology: theory and applications of machining with abrasives, New York: Industrial Press, New York, 2008, pp. 9-59.

[34] J. Chen, Q. Fang, P. Li, Effect of grinding wheel spindle vibration on surface roughness and subsurface damage in brittle material grinding, Int. J. Mach. Tools Manu. 91 (2015) 12-23.

[35] P.V. Krakhmalev, J. Sukumaran, A. Gåård, Effect of microstructure on edge wear mechanisms in WC–Co, Int. J. Refract. Met. H. 25 (2007) 171-178.

[36] K. Wegener, H.W. Hoffmeister, B. Karpuschewski, F. Kuster, W.C. Hahmann, M. Rabiey, Conditioning and monitoring of grinding wheels, CIRP Ann. - Manuf. Technol. 60 (2011) 757-777.

[37] I.D. Marinescu, M. Hitchiner, E. Uhlmann, W.B. Rowe, I. Inasaki, Handbook of machining with grinding wheels, CRC Press, Florida: Boca Raton; 2007, pp. 12-13..

[38] B. Zhang, F. Yang, J. Wang, Z. Zhu, R. Monahan, Stock removal rate and workpiece strength in multi-pass grinding of ceramics, J. Mater. Process. Technol. 104 (2000) 178-184.

[39] I.D. Marinescu, H.K. Tönshoff, I. Inasaki, Handbook of ceramic grinding and polishing, Park Ridge, William Andrew Publishing, Norwich, New York, 2000, pp. 190-199.

[40] L. Ma, Y. Gong, X. Chen, Study on surface roughness model and surface forming mechanism of ceramics in quick point grinding, Int. J. Mach. Tools Manu. 77 (2014) 82-92.

[41] R. Snoeys, J. Peters, A. Decneut, The significance of chip thickness in grinding, CIRP Ann. - Manuf. Technol. 23 (1974) 227-237.

[42] B. Guo, Q. Zhao, H. Li, Ultraprecision grinding of TiC-based cermet hemisphere couples, Int. J. Adv. Manuf. Technol. 73 (2014) 1281-1289.

[43] X. Sun, D.J. Stephenson, O. Ohnishi, A. Baldwin, An investigation into parallel and cross grinding of BK7 glass, Precis. Eng. 30(2006) 145-153.

[44] J.E. Mayer Jr., G.P. Fang, R.L. Kegg, Effect of grit depth of cut on strength of ground ceramics, CIRP Ann. - Manuf. Technol. 43 (1994) 309-312.

[45] H.G. Wobker, H.K. Tonshoff, High-efficiency grinding of structural ceramics, NIST Spec. Publ. 847

(1993) 171.

[46] C.F. Cheung, W.B. Lee, A multi-spectrum analysis of surface roughness formation in ultra-precision machining, Precis. Eng. 24 (2000) 77-87.

[47] C.F. Cheung, W.B. Lee, Characterisation of nanosurface generation in single-point diamond turning, Int. J. Mach. Tools Manu. 41 (2001) 851-875.

[48] Z. Xie, R.J. Moon, M. Hoffman, P. Munroe, Y. Cheng, Role of microstructure in the grinding and polishing of α-sialon ceramics, J. Eur. Ceram. Soc. 23 (2003) 2351-2360.